

# Age patterns in a sample of spiral galaxies

M. C. Sánchez-Gil<sup>1</sup>, H. Jones<sup>2</sup>, E. Pérez<sup>1</sup>, J. Bland-Hawthorn<sup>3</sup>, E. J. Alfaro<sup>1</sup>,  
and J. O’Byrne<sup>3</sup>

<sup>1</sup>Instituto de Astrofísica de Andalucía, Glorieta de la Astronomía s/n, Apto. 3004, 18080 Granada, Spain

<sup>2</sup>Anglo-Australian Observatory, PO Box 296, Epping, NSW 2121, Australia

<sup>3</sup>Sydney Institute for Astronomy, School of Physics, University of Sydney, NSW 2006, Australia

## Abstract

We present the burst ages for young stellar populations in a sample of 6 nearby spiral galaxies using a differential pixel-by-pixel analysis of the ionized gas emission. We explore a new approach for connecting large-scale dynamical mechanisms with star formation processes in disk galaxies, based on burst ages derived from the H $\alpha$  to far UV (FUV) flux ratio. Images of each galaxy in H $\alpha$  were taken with Taurus Tunable Filter (TTF) and matched to FUV imaging from GALEX. The resulting flux ratio provides a robust measure of *relative* age across the disk which we discuss in terms of the large-scale dynamical motions. Systematic effects, such as a variable initial mass function (IMF), non-solar metallicities, variable star-formation history (SFHs), and dust attenuation, have been considered insofar as the models have permitted. The resulting age maps show age gradients along the spiral arms, in addition to circumnuclear regions (M94) or in HII complexes (IC 2574) in specific cases. Remarkably, in the case of M51 we find evidence for a stellar age gradient along short spurs of dust lane branching off the main spiral arms. We find that a comparison of the H $\alpha$  and FUV observations of nearby spiral galaxies is a relatively direct way to probe burst age variations in spirals.

## 1 Introduction

Star formation (SF) activity in galaxies is influenced by many factors, including gas content, mass and dynamical environment [15]. However, the widely-used SF calibrators that linearly relate H $\alpha$  emission or UV flux of a source to its current star formation rate (SFR), are based on simple SF models that neglect environmental factors affecting stellar evolution [14, 19]. Such factors include SF driven by tidal forces instead of bars, and flocculent (as opposed to dominant) spiral arms. Spatial variation in the current SFR and SFH across a galaxy can provide vital clues to its dynamical and secular evolution.

The most common SF diagnostics use far ultra-violet (FUV), far-infrared (FIR), or nebular recombination lines [15]. UV emission is mainly dominated by O-B type stars, with lifetimes  $\lesssim 10^8$  yr [13, 15]. In contrast, the H $\alpha$  line is strong only in the presence of the most massive, hot O stars (masses  $> 10 M_{\odot}$ , ages  $< 20$  Myr) that have enough energy to ionize the surrounding hydrogen. These stars have even shorter lifetimes ( $\lesssim 10^7$  yrs [13, 15]) as they quickly evolve to red supergiants or erupt as supernovae, making the resulting H $\alpha$  emission the most instantaneous probe of SF.

The ratio of the UV and H $\alpha$  fluxes would give a good relative indicator of recent SFH. As a nascent star forming region evolves, the H $\alpha$  line emission declines earlier than the UV continuum, leading to a decrease in the H $\alpha$ /UV ratio. With the appropriate assumptions about the amount of extinction by dust and the nature of the initial mass function (IMF), this ratio is a direct indicator of the age of a new star forming region. Various authors have pointed to other factors that could influence H $\alpha$ /FUV flux ratio, such as variations in the IMF, SFH, and metallicity (e.g. [13, 21, 17]). Different levels of dust attenuation between individual HII regions also has a major influence, especially in the highly extinguished FUV region. Clearly, any effort to use H $\alpha$ /FUV fluxes needs to account for these systematics insofar as the data allow.

Traditionally, comparisons between star forming distributions have concentrated on identifying HII regions and gas clouds – usually by selecting HII regions by eye (e.g. [1, 15]). However, such techniques are necessarily subjective and are therefore difficult to standardize between different authors, data sets, and methodology. By avoiding the need to explicitly define HII regions at all, one removes a major source of systematic error. To this end, recent work has moved towards pixel-by-pixel differential comparisons (e.g. [10]), providing information on the global SF properties of a galaxy without the need to define HII regions.

## 2 Sample and data

The galaxies in our sample were selected across a range of star-forming types by their orientation, proximity, and availability of existing ultraviolet (UV) and far-infrared (FIR) data. Members were chosen to be as near to face-on as possible to mitigate the effects of extinction and scattering, as well as minimizing the wavelength shift in H $\alpha$  due to galactic rotation. Galaxies were also chosen to be close enough ( $\lesssim 10$  Mpc) to have sufficient spatial resolution to see detail in individual SF structures within spiral arms. A summary of their main properties is presented in Table 1.

Optical images were obtained in H $\alpha$  using the Taurus Tunable Filter (TTF [2]) on the William Herschel Telescope (WHT) on 1999 March 4–6. The UV images come from the Nearby Galaxies Survey of the Galaxy Evolution Explorer (NGS survey, GALEX<sup>1</sup>) mission. This survey contains well-resolved imaging (1.5 arcsec/pix), in two passbands: a narrower far-ultraviolet band (FUV;  $\lambda_{\text{eff}}/\Delta\lambda = 1516/268 \text{ \AA}$ ), and a broader near-ultraviolet band (NUV;  $\lambda_{\text{eff}} = 2267/732 \text{ \AA}$ ).

---

<sup>1</sup><http://galex.stsci.edu>

Table 1: Galaxy Parameters (from NASA Extragalactic Database)

Galaxy	RA (J2000) h m s	Dec. (J2000) ° ' "	Type	Dist. (Mpc)	Inclin. (deg)	Dimensions (arcmin)	$M_B$
NGC 628 (M74)	01 36 41.70	+15 46 59.4	SA(s)c	11.4	5	10.5×9.5	9.95
IC 2574	10 28 21.25	+68 24 43.2	SAB(s)m	4.0	77	13.2×5.4	10.80
NGC 4321 (M100)	12 22 54.90	+15 49 21.0	SAB(s)bc	16.1	30	7.4×6.3	10.05
NGC 4736 (M94)	12 50 53.06	+41 07 13.7	(R)SA(r)ab	4.7	35	11.2×9.1	8.99
NGC 5055 (M63)	13 15 49.25	+42 01 49.3	SA(rs)bc	8.4	55.2	12.6×7.2	9.31
NGC 5194 (M51a)	13 29 52.71	+47 11 42.6	SA(s)bc pec	8.1	20	11.2×6.9	8.96

Archival SPITZER<sup>2</sup> images for the galaxies of the sample were used to provide additional estimates of extinction. Images at 24, 70, and 160  $\mu\text{m}$  for each galaxy were combined into an image of total far-infrared flux, according to  $F_{\text{TIR}} = \zeta_1 \nu F_\nu(24 \mu\text{m}) + \zeta_2 \nu F_\nu(70 \mu\text{m}) + \zeta_3 \nu F_\nu(160 \mu\text{m})$ , where  $[\zeta_1, \zeta_2, \zeta_3] = [1.559, 0.7686, 1.347]$  [8]. The different plate scales for each frame (1.5 "/pix for 24  $\mu\text{m}$ , 4.5 "/pix for 70  $\mu\text{m}$ , and 9 "/pix for 160  $\mu\text{m}$ ) were all resampled to 1.5 "/pix where necessary, identical to that of the optical (0.56 arcsec/pix) and GALEX (FUV and NUV) frames. Once we resample and align our H $\alpha$ , UV, and FIR images data onto a common pixel scale and orientation (north-up east-left), the pixel-by-pixel technique becomes straightforward to implement.

The extinction within our galaxy is corrected using the [25] dust maps<sup>3</sup> which measure the Galactic extinction in all directions. The internal reddening is corrected using a straight relation between the  $A_{\text{FUV}}$  extinction factor and the TIR-to-FUV flux ratio, from [5],

$$A_{\text{FUV}} = -0.0333y^3 + 0.3522y^2 + 1.1960y + 0.4967, \quad (1)$$

with  $y = \log(F_{\text{dust}}/F_{\text{FUV}})$ . The  $F_{\text{TIR}}/F_{\text{FUV}}$  ratio is a robust and universal tracer of dust extinction, almost independent of the dust/stars geometry and of the dust properties, provided that the galaxies are actively forming stars [3, 4, 11]. The  $A(\text{H}\alpha)$  extinction factor is calculated through the relation  $A_{\text{FUV}} = 1.4 A(\text{H}\alpha)$ .

### 3 Stellar population modelling and ages

Model H $\alpha$  and FUV luminosities were generated from Starburst99 [18]. The code can be run with two different star formation modes, an instantaneous burst of star formation and star formation proceeding continuously at a constant rate. For each mode of SF, there are three choices for the stellar initial mass function, IMF. The reference model is a power law with exponent  $\alpha = 2.35$ , with low-mass and high-mass cutoff  $M_{\text{low}} = 1 M_\odot$  and  $M_{\text{up}} = 100 M_\odot$ , respectively. An IMF with  $\alpha = 3.3$ , between  $1 M_\odot$  and  $100 M_\odot$ , and finally a truncated Salpeter IMF:  $\alpha = 3.3$ , with  $M_{\text{low}} = 1 M_\odot$  and  $M_{\text{up}} = 30 M_\odot$ . Five metallicities are available for each model:  $Z = 0.040, 0.020$ , (solar,  $Z_\odot$ ), 0.008, 0.004 and 0.001 (see Table 1 of [18]).

<sup>2</sup><http://irsa.ipac.caltech.edu/data/SPITZER/SINGS/summary.html>

<sup>3</sup><http://www.astro.princeton.edu/~schlegel/dust/data/data.html>

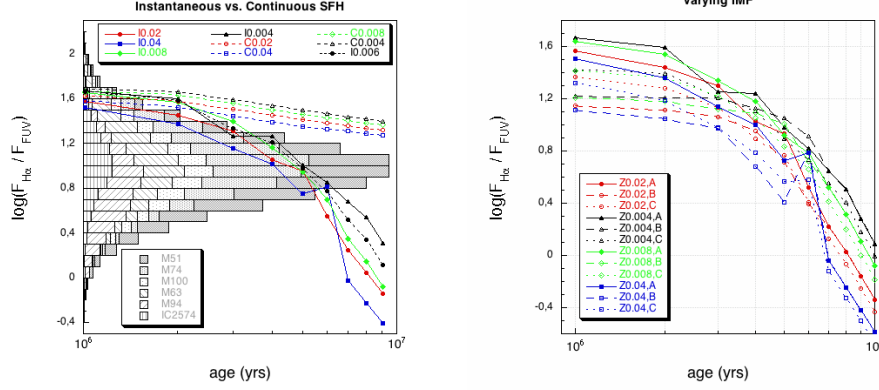


Figure 1: *Left*: Histograms of the observed H $\alpha$  to FUV flux ratios for the galaxy sample, compared with the SB99 models for the instantaneous (I) and continuous (C) SF law, with Salpeter IMF and different metallicity values. *Right*: H $\alpha$  to FUV flux ratio models for different IMFs: (A) (Salpeter)  $\alpha = -2.35$  and  $M_{\text{up}} = 100 M_{\odot}$ ; (B)  $\alpha = -2.35$ ,  $M_{\text{up}} = 30 M_{\odot}$ ; (C)  $\alpha = -3.3$ ,  $M_{\text{up}} = 100 M_{\odot}$ . Instantaneous SF law, and same metallicity color code.

The models cover the age range  $10^6$ – $10^9$  yr, and the SED cover the wavelength range from  $100 \text{ \AA}$  to  $1 \mu\text{m}$ . We only keep the *age range* from 1 to 10 Myr, since we are only interested in young stellar populations who dominate the H $\alpha$  and UV emission; H $\alpha$  emission is negligible for ages  $> 10$  Myr.

We chose the instantaneous star formation law, since it is more sensitive to the age variation in the younger star forming regions, as we can see in Fig. 1 (top left). The predicted H $\alpha$ /FUV flux ratios modeled by SB99 are in agreement with the observed range of values when an instantaneous SF law is applied. Despite this oversimplified approach to the SFH, expected to be more complex, because we are concerned with local regions of star formation, younger than  $10^8$  yr, and not integrating luminosities over the entire disk, an instantaneous starburst can represent them reasonably well (e.g., [23, 13]).

## 4 Age maps

The age maps for all the galaxies of our sample are plotted in Fig. 2. The free parameters used for these age maps are instantaneous SF law, Salpeter IMF and solar metallicity (based on radial oxygen abundance by [24]). For IC 2574 [22] give a  $\sim 30\%$  solar metallicity, so we use the interpolated value  $Z = 0.006$ .

The resulting age maps show age patterns across these nearby and resolved galaxies, remarking as well their morphology and in many cases finding interesting age gradients. This is a common characteristic found, the observation of age gradients along or across either the

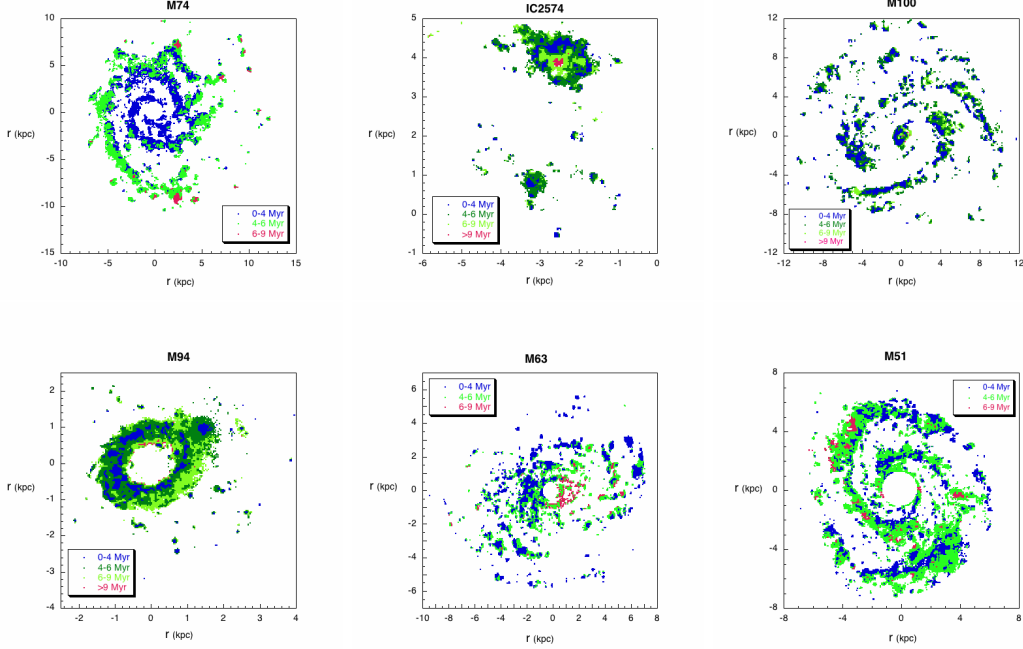


Figure 2: Age maps for the galaxies of our sample, and for the default parameters of the model: instantaneous star formation law, Salpeter IMF  $\alpha = 2.35$ ,  $M_{\text{up}} = 100 M_{\odot}$  and solar metallicity except for IC 2574, where a interpolation between  $Z = 0.004$  and  $Z = 0.008$  calibration curves is applied. Each age group is represented with a different color, indicated in each case in the panel. The axis are the relative position to the center of the galaxy, in kpc units.

spiral arms, for the grand-design spiral galaxies, or in circumnuclear regions (M94) and in irregular HII regions (IC 2574). For M94 and IC 2574 secondary SF is observed in the rims of the primary one, probably triggered by the latter. For M63 the age gradient happens overall the galactic disk, being an outstanding feature as the eastern side is dominated by the younger population ( $< 4$  Myr), whereas in the inner  $\pm 3$  kpc of the western side the older population (6–9 Myr) dominates. Similarly in M74, there are age gradients across its spiral arms and an increasing age gradient from the inner to the outer parts of the galaxy. This corresponds with a very strong  $H\alpha$  emission in the inner part of this galaxy. In the case of M51, a remarkable result is the connection found between the age gradients across the spiral arms with the spurs in this galaxy.

## 5 Reliability and robustness of the method

The photometric uncertainty on the  $F_{H\alpha}/F_{\text{FUV}}$  flux ratio is dominated by the error on the FUV flux (15 to 25%) and not  $H\alpha$  ( $< 5\%$ ). An additional error term comes from the use of

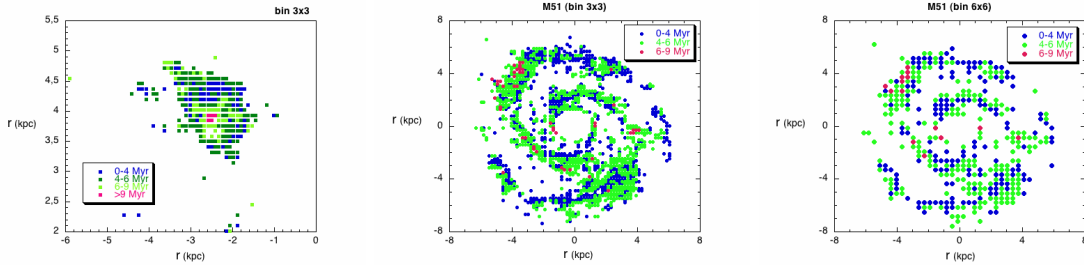


Figure 3: Age maps obtained after binning the galaxy images. The axis are the radius to the galactic center, in kpc units. *Left*: the pixel by pixel age map of IC 2574, zoomed at the northeastern stellar complex. *Center and right*: age maps for M51 after the  $3 \times 3$  and  $6 \times 6$  binnings.

Eq. 1 for the FUV extinction correction, which depends on the uncertainties in the FIR. The uncertainties for the  $24 \mu\text{m}$ ,  $70 \mu\text{m}$  and  $160 \mu\text{m}$  are 4%, 7% and 12% respectively [9], implying 15% uncertainty overall in the  $F_{\text{TIR}}$  and 30% in the  $F_{\text{H}\alpha}/F_{\text{FUV}}$  ratio.

Photometric uncertainties aside, the age-dating technique is subject to a number of potential sources of systematic error (e.g. [13, 21, 17]). We test the robustness of our results to systematic error by varying the assumptions we have made over a plausible range of values. Specifically, the effects we examine are: (i) the lowest limit on cluster mass allowable for our assumptions on ionizing flux, (ii) the effect of changing the spatial bin size, and (iii) the effect of changes to the metallicity and IMF assumptions in the model. We deal with each of these in turn:

(i) All the galaxies, except the irregular IC 2574, have pixel stellar masses greater than  $10^4 M_{\odot}$ , clearly above any lower mass limit  $M^{\text{min}}$  given by [6]. Below this limit the cluster should be better modeled by a single star instead of a star cluster. After a  $3 \times 3$  pix binning the pixel masses of IC 2574 keep above the  $10^4 M_{\odot}$  mass limit, and the binned age map shows the same age pattern that the pixel by pixel one (c.f. left panel of Fig. 3).

(ii) The use of the pixel by pixel technique raises the issue of the validity of assuming that for a given pixel the relationship between the  $\text{H}\alpha$  emission and the ultraviolet emission of that pixel correspond to the assumption made in the models, i.e., that the ionization in that pixel corresponds to the same stars producing the UV flux. By performing a spatial binning with different bin sizes in the  $\text{H}\alpha$  and in the UV images we can check whether the resulting age maps produce a consistent result (Fig. 3).

(iii) The uncertainties in the  $F_{\text{H}\alpha}/F_{\text{FUV}}$ , both from the models and the flux measurement errors, and affecting the resulting age assignment to a star forming region, are summarized at once in a single figure, by means of uncertainty and confidence maps (Fig. 4).

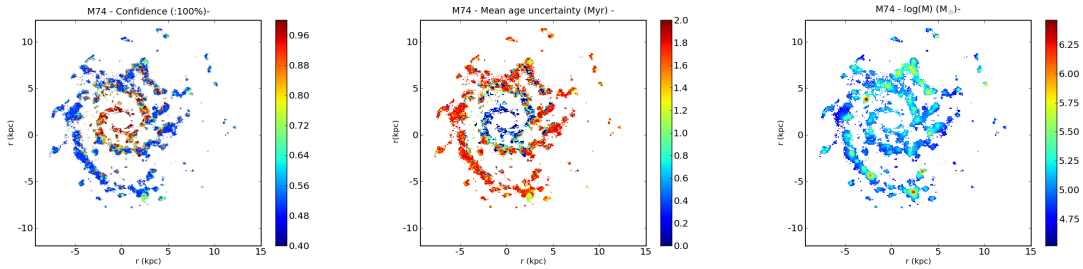


Figure 4: *Left*: Confidence map. The confidence in the age assignment, among the different possible SB99 models and between the flux ratio uncertainty, measured as the probability. *Center*: Uncertainty map, given in terms of the average uncertainty on age, in Myr. *Right*: Mass map. The lower mass limit calculated via linearly scaling the extinction-corrected observed  $L_{\text{FUV}}$  with the model.

## 6 Summary

The study of the SFH and SFR provides vital information regarding the evolutionary properties of galaxies and the physical processes which drive their evolution. SF can vary across the different types of galaxies depending on factors such as gas content, mass, or environment [15], even for the same morphological type [12].

The proposed method is based on the interaction of stars and gas as a probe of star formation mechanisms, that helps understanding the star formation processes and the propagation of the star formation process. We obtain 2D age maps from the comparison between the UV and  $\text{H}\alpha$  emission in nearby and spatially resolved galaxies. This work shows that a comparison of the  $\text{H}\alpha$  and FUV observations of nearby spiral galaxies is a relatively direct way to probe burst age variations in spirals.

The use of a pixel-wise age dating technique allows age mapping of the youngest stellar population present at each pixel, without any a priori assumptions about the spatial distribution of the star forming regions. The technique allows the spatial characterization of the age distribution for HII regions within a range of distance in the Local Volume, that provides enough spatial resolution to infer the internal SFH processes.

These age maps provide a global view of the SF processes taking place in the galactic disks, the maximum scale of coherent star formation, its relation with other large scale processes of star formation in galaxies, such as density waves and, as it is the case for M51, mapping the relationship between star formation and dynamics.

## Acknowledgments

This work is part of the PhD dissertation of M. Carmen Snchez-Gil, funded by the Spanish Ministerio de Ciencia e Innovación (MICINN), under the FPU grant AP-2004-2196. We acknowledge financial support from Spanish MICINN through grants AYA2007-64052 and AYA2007-64712 and from Consejería de Educación y Ciencia (Junta de Andalucía) through TIC-101, TIC-4075 and TIC-114.

## References

- [1] Battinelli, P., Capuzzo-Dolcetta, R., Hodge, P. W., Vicari, A., & Wyder, T. K. 2000, *A&A*, 357, 437
- [2] Bland-Hawthorn, J., & Jones, D. H. 1997, *The Hubble Space Telescope and the High Redshift Universe*, 121
- [3] Buat, V., & Xu, C. 1996, *A&A*, 306, 61
- [4] Buat, V., Donas, J., Milliard, B., & Xu, C. 1999, *A&A*, 352, 371
- [5] Buat, V., et al. 2005, *ApJL*, 619, L51
- [6] Cerviño, M., Luridiana, V., Pérez, E., Vílchez, J. M., & Valls-Gabaud, D. 2003, *A&A*, 407, 177
- [7] Cortese, L., et al. 2006, *ApJ*, 637, 242
- [8] Dale, D. A., & Helou, G. 2002, *ApJ*, 576, 159
- [9] Dale, D. A., et al. 2007, *ApJ*, 655, 863
- [10] Eskridge, P. B., et al. 2003, *ApJ*, 586, 923
- [11] Gordon, K. D., Clayton, G. C., Witt, A. N., & Misselt, K. A. 2000, *ApJ*, 533, 236
- [12] Grebel, E. K. 2000, *Star Formation from the Small to the Large Scale*, 445, 87
- [13] Iglesias-Páramo, J., Boselli, A., Gavazzi, G., & Zaccardo, A. 2004, *A&A*, 421, 887
- [14] Kennicutt, R. C., Jr. 1983, *ApJ*, 272, 54
- [15] Kennicutt, R. C., Jr. 1998, *ApJ*, 498, 541
- [16] Kennicutt, R. C., Jr., et al. 2003, *PASP*, 115, 928
- [17] Lee, J. C., et al. 2009, *ApJ*, 706, 599
- [18] Leitherer, C., et al. 1999, *ApJS*, 123, 3
- [19] Madau, P., Ferguson, H. C., Dickinson, M. E., Giavalisco, M., Steidel, C. C., & Fruchter, A. 1996, *MNRAS*, 283, 1388
- [20] Martin, C. L., & Kennicutt, R. C., Jr. 2001, *ApJ*, 555, 301
- [21] Meurer, G. R., et al. 2009, *ApJ*, 695, 765
- [22] Miller, B. W., & Hodge, P. 1996, *ApJ*, 458, 467
- [23] Pasquali, A., et al. 2008, *ApJ*, 687, 1004
- [24] Pilyugin, L. S., Vílchez, J. M., & Contini, T. 2004, *A&A*, 425, 849
- [25] Schlegel, D. J., Finkbeiner, D. P., & Davis, M. 1998, *ApJ*, 500, 525
- [26] Tonry, J. L., Dressler, A., Blakeslee, J. P., Ajhar, E. A., Fletcher, A. B., Luppino, G. A., Metzger, M. R., & Moore, C. B. 2001, *ApJ*, 546, 681